Nanoscale

Accepted Manuscript

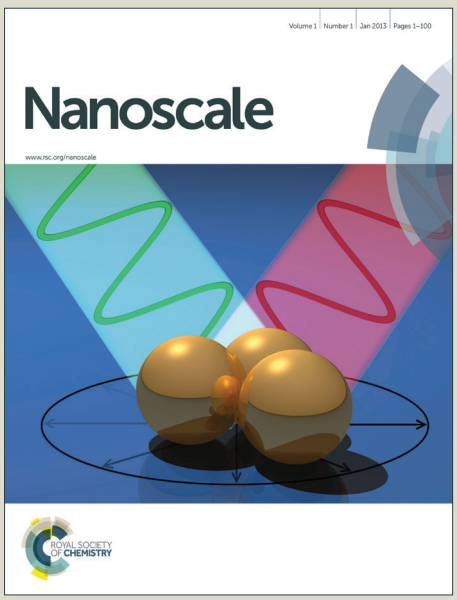

ROYAL SOCIETY OF CHEMISTRY

www.rsc.org/nanoscale

Cite this: DOI: 10.1039/c0xx00000x

www.rsc.org/xxxxxx

ARTICLE TYPE

Self-assembly and optical properties of porphyrin-based amphiphile

Ruijiao Dong,[a] Yang Bo,[§b] Gangsheng Tong,[b] Yongfeng Zhou,[a] Xinyuan Zhu*[a] and Yunfeng Lu*[a,c]

Received (in XXX, XXX) Xth XXXXXXXXX 20XX, Accepted Xth XXXXXXXXX 20XX
DOI: 10.1039/b000000x

A porphyrin-based amphiphile that exhibits various self-assembled nanostructures in different solvents, has been successfully prepared. The effect of aggregated structure on optical properties of this amphiphile has been well investigated. Furthermore, this porphyrin-based amphiphile and its assemblies show dynamic/reversible variations in morphology and optical properties in response to light.

Owing to their attractive photophysical, photochemical, and electronic properties, the porphyrin-based nanomaterials with well-defined architecture and excellent optical performance have received much attention in a wide range of fields including photodynamic therapy, molecular electronics, photonics as well as light-energy conversion.[1] Over the past few decades, a great number of porphyrin-based nanomaterials with various forms such as nanoparticles,[2] nanovesicles,[3] nanosheets,[4] nanorods,[5] nanofibers,[6] nanobelts[7] and nanotubes,[8] have been designed and developed via molecular self-assembly by employing noncovalent interactions including electrostatic force, metal-ligand coordination, π-π stacking, hydrogen bonding as well as host-guest interaction. For example, the group of Shelnutt reported robust porphyrin nanotubes[8a] as well as microscale donor/acceptor biomorphs[9] by ionic self-assembly of two oppositely charged porphyrins in aqueous solution. Parquette and coworkers[8b] successfully acquired a donor/acceptor nanotube with bicontinuous arrays from the self-assembly of a porphyrin-based bola-amphiphile via extensive intermolecular π-π interaction. Jayawickramarajah et al.[6c] developed a convenient approach for the self-assembly of well-defined porphyrin nanowires in water using robust β-cyclodextrin/adamantane host/guest interaction. Very recently, Zhang et al.[10] reported a novel porphyrin-based supramolecular photosensitizer based on host/guest interaction, which showed a greatly improved antibacterial efficiency. Generally speaking, great progress has been made in porphyrin-based material chemistry, and various self-assembly strategies for well-defined porphyrin-based nanostructures have been well established. However, hitherto, most of these studies have mainly focused on the design and construction of various porphyrin-based nanostructures with well-defined morphologies, and few studies devoted to expatiating on the effect of aggregated structure on optical properties. Therefore, to push forward the development of porphyrin chemistry, it is necessary to explore the relationship of aggregated structure and optical behavior of porphyrin-based nanomaterials.

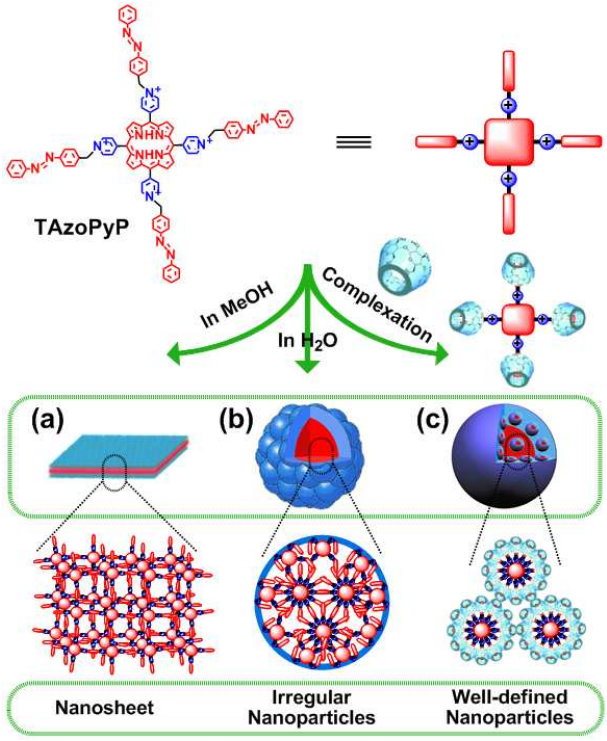

Scheme 1. Schematic representation of the chemical structure of TAzoPyP and the resulting aggregates under different conditions: (a) nanosheet for TAzoPyP in MeOH, (b) irregular nanoparticles for TAzoPyP in water and (c) well-defined nanoparticles for TAzoPyP/α-CD_4 complex in water.

Herein, we report a porphyrin-based amphiphile, which combines a hydrophobic porphyrin core with four hydrophilic quaternary ammonium units and four photosensitive azobenzene (Azo) head groups. As shown in Scheme 1, the porphyrin core unit provides a photoactive and fluorescent functionality, the quaternary ammonium units allow for dispersion in aqueous medium, and the Azo groups endow with a photosensitivity. Owing to its unique chemical structure and amphiphilic nature, the resulting porphyrin-based amphiphile exhibits various morphologies via self-assembly in different solvents, thus bringing on distinct optical properties. Meanwhile, this amphiphile as a multivalent guest is capable of complexing with α-cyclodextrin (α-CD) to form supramolecular inclusion complex, and then further self-organizes into well-defined spherical nanoparticles in aqueous medium accompanied by excellent

optical properties. In addition, this porphyrin-based amphiphile and its assemblies show dynamic/switchable morphology and optical properties in response to light. More importantly, the effect of self-assembly behavior on optical property for this amphiphile has been well investigated so as to get a better understanding on the structure-performance relationship.

The procedures for the synthesis of porphyrin and its derivatives are depicted in Schemes S1-S3 (see ESI†). Firstly, the porphyrin-based amphiphile, 5,10,15,20-*tetra*-(4-*N*-methyl-azobenzene-pyridyl)-porphyrin tetrabromide (TAzoPyP), was designed and synthesized via quaternization reaction between 5,10,15,20-*tetra*-(4-pyridyl)-porphyrin (TPyP) and 4-bromomethyl azobenzene. As a control, the water-soluble porphyrin derivative, 5,10,15,20-*tetra*-(4-*N*-ethylpyridyl)-porphyrin tetraiodide (TEtPyP) was prepared following a synthesis route in Scheme S2. The successful preparation of TAzoPyP and TEtPyP was clearly confirmed by ^{1}H NMR, FTIR, UV-Vis and Q-TOF-MS. The detailed characterization data are described in Figs. S1-S11 (see ESI†).

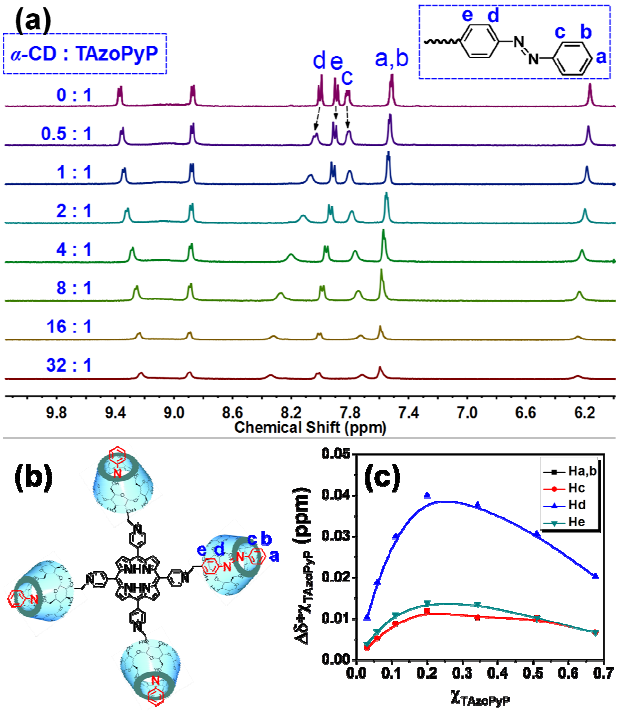

Fig. 1. (a) ^{1}H NMR spectra of α-CD and TAzoPyP at different molar ratios of 0:1, 0.5:1, 1:1, 2:1, 4:1, 8:1, 16:1, and 32:1 in DMSO-d_6/D_2O (1/1, *v*/*v*). The concentration of TAzoPyP was 2 mM. (b) Schematic representation of the formation of TAzoPyP/α-CD_4 supramolecular complex. (c) Job's plot of α-CD and TAzoPyP. $\chi_{TAzoPyP}$ is the molar fraction of TAzoPyP in α-CD/TAzoPyP mixture.

As a multivalent guest, this resulting Azo-modified porphyrin amphiphile (TAzoPyP) is exactly capable of multivalently binding to some macrocyclic compounds (e.g., α-CD) to form supramolecular complex. Thus, the host/guest property of TAzoPyP and α-CD was investigated by using UV-Vis spectroscopy and ^{1}H NMR analysis. Firstly, the association intensity for the model compounds of Azo and α-CD was evaluated by using UV-Vis spectroscopy. According to the modified Hildebrand-Benesi equation,[11] the association constant for the 1/1 inclusion complex of the Azo guest with α-CD host in MeOH/H_2O (1/1, v/v) was calculated to be 1.84×10^4 M^{-1} (Fig. S12, see ESI†). Furthermore, the binding stoichiometry of TAzoPyP to α-CD was determined by ^{1}H NMR analysis. In Fig. 1a, the chemical shift of the Azo protons (Ha-e) of TAzoPyP gradually increases with the molar ratio of α-CD/TAzoPyP from 0/1 to 32/1, implying the inclusion complexation of TAzoPyP with α-CD. Following a Job's plot of $\Delta\delta^*\chi_{TAzoPyP}$ *vs.* $\chi_{TAzoPyP}$ in Fig. 1c, the maximum value is found to be around 0.2, which indicates that the binding stoichiometry of TAzoPyP to α-CD is 1/4. Therefore, the above results exactly demonstrate the formation of TAzoPyP/α-CD_4 inclusion complex (Fig. 1b).

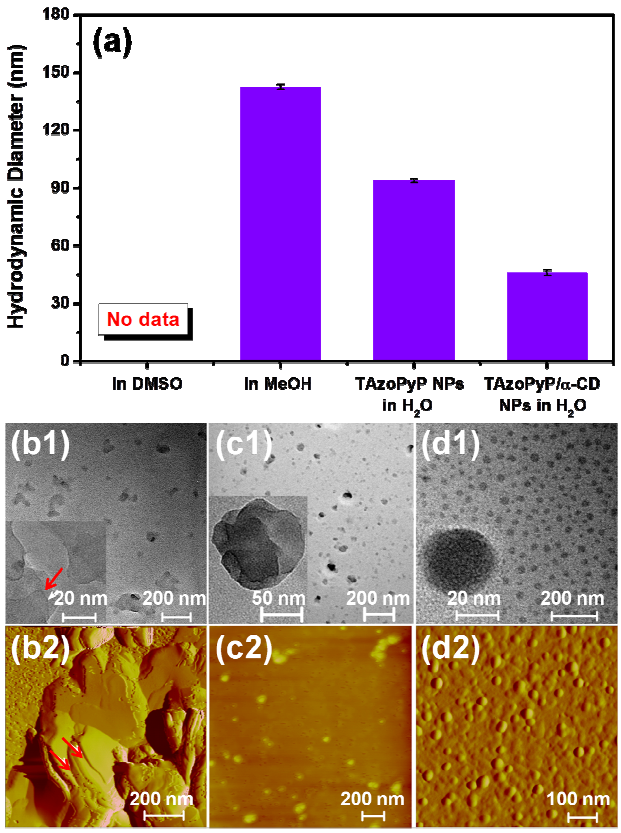

Fig. 2. (a) The hydrodynamic diameter of TAzoPyP in different solvents with the same TAzoPyP concentration of 0.2 mg/mL. (b1-d1) TEM images and (b2-d2) AFM images of (b) TAzoPyP in MeOH, (c) TAzoPyP nanoparticles (TAzoPyP NPs) and (d) TAzoPyP/α-CD_4 supramolecular nanoparticles (TAzoPyP/α-CD NPs). The insets in (b1, c1, d1) are magnified images. Black bars represent the mean values (n = 5). The red arrows in (b1, b2) indicate the lamellar structure.

Interestingly, this porphyrin-based amphiphile (TAzoPyP) presents distinct aggregated morphologies in some solvents due to its unique chemical structure. The morphology and size of the aggregates were investigated by dynamic laser scattering (DLS), transmission electron microscopy (TEM), and atomic force microscopy (AFM) measurements. In Fig. 2a, no apparent aggregates can be observed when TAzoPyP is dissolved in dimethyl sulfoxide (DMSO), suggesting that TAzoPyP displays predominantly unimolecular structures in DMSO. Interestingly, TAzoPyP can directly disperse in methanol (MeOH) to form a large amount of aggregates with an average hydrodynamic

diameter (D_h) of 142.5±1.3 nm. The TEM image in Fig. 2b1 shows sheet-like assemblies with an average size of approximate 130 nm. Such a lamellar structure is clearly presented in the inset of Fig. 2b1. Meanwhile, the AFM image in Fig. 2b2 further confirms the formation of the lamellar structure. Because of its amphiphilic nature, TAzoPyP tends to self-assemble in aqueous medium via hydrophobic interaction. Both TEM and AFM images in Figs. 2c1-2c2 exhibit irregular spherical nanoparticles with a mean size of *ca*. 80 nm based on 100 individual nanoparticles from TEM image, which is consistent with the D_h of 93.8±1.1 nm determined by DLS (Fig. 2a). The inset in Fig. 2c1 presents slightly corrugated spherical surfaces as a result of disordered stacking of this rigid amphiphile in water.

In addition, TAzoPyP/α-CD_4 supramolecular complex as an amphiphilic molecule can self-assemble in water to form morphologically distinct aggregates. TEM image in Fig. 2d1 evidently demonstrates that the self-assemblies are homogeneous spherical nanoparticles according to a slight difference between the particle skin and the inner pool. Such a well-defined spherical structure is clearly presented in the inset of Fig. 2d1. A large number of nanoparticles with uniform size can also be observed as shown in the large scale TEM image (Fig. S13, see ESI†). Also, AFM image in Fig. 2d2 confirms the uniform spherical structures. Both of TEM image (Fig. 2d1) and AFM image (Fig. 2d2) show that the statistical size of the nanoparticles is approximate 35 nm, which is consistent with the D_h of 46.0±1.4 nm determined by DLS (Fig. 2a). Besides, zeta potential measurement was performed to assess the surface charge density of these two nanoparticles through aqueous self-assembly of TAzoPyP and its supramolecular complex. In Fig. S14 (see ESI†), TAzoPyP/α-CD_4 supramolecular nanoparticles (TAzoPyP/α-CD NPs) exhibit relatively lower zeta potential value (17.4±0.66 mV) than that of TAzoPyP nanoparticles (TAzoPyP NPs) (23.4±0.69 mV), which might be attributed to the shielding effect of α-CD. By comparison, the supramolecular nanoparticles are much more stable than TAzoPyP NPs, and they can be kept in water without any changes in morphology and size for at least half a year.

Moreover, the molecular packing structures in these aggregates were investigated by UV-Vis absorption spectroscopy, circular dichroism (CD) spectroscopy and fluorescence excitation spectroscopy. As depicted in Fig. 3a, TAzoPyP in DMSO exhibits three absorption bands at *ca*. 330 nm ascribed to the π-π* transition of Azo group as well as at *ca*. 430 nm and from 500 to 650 nm corresponding to Soret band and Q band for the porphyrin chromophore, whereas TEtPyP in DMSO just exhibits two absorption bands at *ca*. 430 nm and from 500 to 650 nm corresponding to Soret band and Q band for the porphyrin chromophore (Fig. S15, see ESI†). In Fig. 4a, the small shoulder at around 433 nm for TAzoPyP in DMSO reflects the occurrence of a small amount of aggregation, which further confirms that TAzoPyP in DMSO mainly exists in the form of unimolecular state. In MeOH, the UV adsorption bands for both of the π-conjugated Azo and porphyrin chromophores in TAzoPyP show a slight blue shift (< 10 nm) compared with that in the good solvent of DMSO (Fig. 3a), indicating that TAzoPyP adopts a H-type aggregation in the lamellar aggregates.[12] However, since this blue shift of the UV absorption bands of the Azo and porphyrin chromophores is relatively small, it implies that the TAzoPyP in the nanosheets could be arranged in an incompact and less optimal way of H-aggregation. It might be attributed to the fact that the π-π interaction between TAzoPyP molecules was greatly suppressed by the intermolecular electrostatic interaction, resulting in the formation of the incompact aggregated structure. Based on these data, we proposed a lamellar self-assembly mechanism for TAzoPyP in MeOH as shown in Scheme 1a.

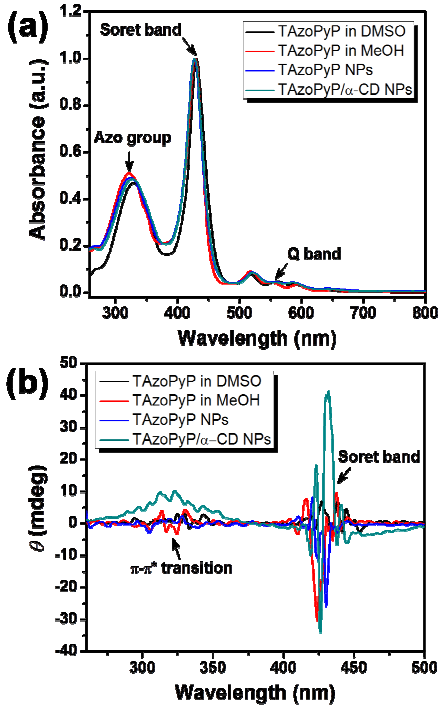

Fig. 3. (a) Normalized UV-Vis spectra and (b) circular dichroism (CD) spectra of TAzoPyP in DMSO, TAzoPyP in MeOH, TAzoPyP NPs and TAzoPyP/α-CD NPs.

Likewise, the formation of the irregular spherical nanoparticles for TAzoPyP in water was accompanied by slight and narrow blue-shifted peaks (Fig. 3a). Blue-shifting of the Azo band (324 nm) and porphyrin Soret band (427 nm) in water is consistent with the presence of H-type π-π interaction of both the Azo and porphyrin chromophores within the nanoparticles. As further evidence, the appearance of a new excitation peak at *ca*. 438 nm (Fig. 4a) demonstrates the formation of a large number of aggregates in water. Also, TAzoPyP is found to be a non-planar molecule according to the molecular simulation in Fig. S16 (see ESI†). Therefore, it is incapable of orderly stacking in aqueous medium via hydrophobic interactions. In Fig. 3b, no circular dichroism (CD) signals are present for TAzoPyP in DMSO, while only the porphyrin Soret band exhibits an excitonic couplet at *ca*. 430 nm of the CD spectrum for TAzoPyP in water that produces irregular spherical aggregates as observed by TEM and AFM (Fig. 2c). The lack of any Azo related peaks in the CD spectrum indicates that intermolecular π-π interactions of porphyrin moiety plays an crucial role in driving assembly under the condition, resulting in relatively disordered Azo segments within the assembly that does not display CD signals. This phenomenon is in good agreement with the proverbial tendency of porphyrin molecules to spontaneously aggregate into disordered materials.[13] Thus, a model for the aqueous self-assembly of TAzoPyP can be

envisaged in Scheme 1b.

In contrast, the resulting well-defined spherical aggregates through aqueous self-assembly of TAzoPyP/α-CD_4 supramolecular complex exhibit extremely tiny blue-shifted peaks (2 nm around) for both the Azo and porphyrin chromophores (Fig. 3a), suggesting that the π-π interaction of TAzoPyP molecules in the nanoparticles are very weak. The observation might be attributed to the following two facts: First, the introduction of α-CD significantly enhances the water-solubility of TAzoPyP to weaken the intermolecular hydrophobic interactions; Second, the host-guest interaction between Azo group of TAzoPyP and α-CD competes with the π-π interaction of Azo groups to prevent further stacking of TAzoPyP in water. In Fig. 3b, the TAzoPyP/α-CD NPs in water produce characteristically distinct CD spectrum compared with those obtained under other conditions. Notably, the CD spectrum of TAzoPyP/α-CD NPs in water shows strong positive excitonic couplets centered at *ca.* 325 and 430 nm, corresponding to Azo π-π* transition and porphyrin (Soret band) transition, respectively. The positive excitonic couplet of Azo groups at *ca.* 325 nm indicates that the Azo moiety of TAzoPyP inserts in the α-CD cavity with its electronic transition moment parallel to the α-CD axis.[14] Thus, the Azo moieties of TAzoPyP could vibrate or rotate along its axis in the nanoparticle. The couplet related to the porphyrin Soret band at *ca.* 430 nm is associated with two quasi-degenerate transitions being oriented perpendicular to each other, implying that rotation of the porphyrin is possible around its two long axes.[15] Accordingly, the multimolecular aggregation model of amphiphilic TAzoPyP/α-CD_4 supramolecular complex is presented in Scheme 1c. In addition, the X-ray diffraction (XRD) analyses were further performed to confirm the lamellar structure for TAzoPyP in MeOH as well as the disordered stacking in these spherical nanoparticles in Fig. S17 (see ESI†).

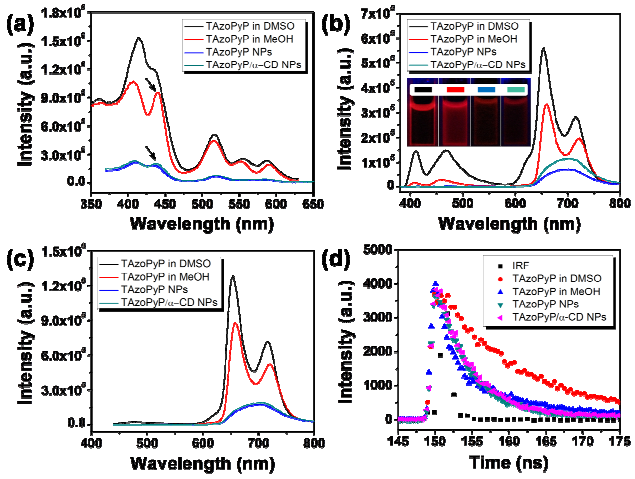

Fig. 4. (a) Fluorescence excitation spectra and (b-c) steady-state fluorescence spectra of TAzoPyP in DMSO, TAzoPyP in MeOH, TAzoPyP NPs and TAzoPyP/α-CD NPs at an excitation wavelength of 360 nm for (b) or 415 nm for (c). The insets in (b) are fluorescent images of the solutions excited with a 365 nm UV lamp. (d) Time-resolved fluorescence spectra of TAzoPyP in DMSO, TAzoPyP in MeOH, TAzoPyP NPs and TAzoPyP/α-CD NPs with excitation at 415 nm and detection at an emission wavelength of 655 nm or 700 nm after proper deconvolution of the instrument response function (IRF). The concentration of all sample solutions is 10 μM.

Next, we attempted to explore the relationship between optical properties and aggregated structures of TAzoPyP under different conditions. The steady-state fluorescence spectroscopy experiment was firstly performed to assess the fluorescence performance of TAzoPyP with various aggregated morphologies. In Fig. 4b, the steady-state fluorescence spectra of TAzoPyP in DMSO and TAzoPyP in MeOH at an excitation wavelength of 360 nm were characterized by four emission bands for the porphyrin moiety at 650 and 715 nm, along with the Azo group at 410 and 470 nm. By comparison, the slight red-shifted bands for porphyrin moiety and slight blue-shifted bands for Azo group can be observed for TAzoPyP in MeOH, which may arise from the lamellar aggregation of TAzoPyP in MeOH. Inversely, the steady-state fluorescence spectra of the aqueous solution of TAzoPyP and TAzoPyP/α-CD just exhibit a single fluorescence emission band centered at around 700 nm in Fig. 4b. The red-shifted fluorescence bands for porphyrin moiety observed here are consistent with the aggregation of TAzoPyP in water.

In contrast to the fluorescence spectrum of the DMSO solution of TAzoPyP, it is noted that the other three aggregated samples display weakened or even undetectable fluorescence bands at 410 and 470 nm for Azo chromophore, which can be mainly attributed to the following fact. As depicted in Fig. S18 (see ESI†), the fluorescence emission peaks of the Azo group overlap the absorption band of the porphyrin moiety perfectly, making it possible for the porphyrin moiety to absorb the fluorescence emitted by the Azo group through fluorescence resonance energy transfer (FRET). Also, the aggregation of TAzoPyP in MeOH and water shortens the intermolecular distance of TAzoPyP to further enhance intermolecular FRET, resulting in significant weakening of fluorescence bands of Azo group. To our knowledge, this is the first report on azobenzene-containing donor-acceptor pairs for FRET up to now. Meanwhile, the TAzoPyP/α-CD NPs exhibit stronger fluorescence than that of TAzoPyP NPs. In our previous report, we found that both the intermolecular aggregation of Azo chromophores[16] and the CD/Azo host/guest interaction[17] could greatly enhance the fluorescence of Azo chromophores. As a result, the enhanced Azo fluorescence can be effectively absorbed by the porphyrin moiety via intermolecular FRET process, which leads to an increase in the fluorescence. In addition, the TAzoPyP solutions with different aggregated morphologies under UV light (365 nm) irradiation exhibit distinct fluorescent colors: reddish-brown for TAzoPyP in DMSO, bright red for TAzoPyP in MeOH as well as dark red for TAzoPyP NPs and TAzoPyP/α-CD NPs (the inset of Fig. 4b).

In Fig. 4c, the steady-state fluorescence spectra of TAzoPyP in DMSO and TAzoPyP in MeOH upon direct excitation of the porphyrin moiety at 415 nm just present two diagnostic fluorescence emission bands for the porphyrin moiety at 650 and 715 nm, while only single fluorescence emission peak can be observed for TAzoPyP NPs and TAzoPyP/α-CD NPs in water. By comparison with TAzoPyP in DMSO, TAzoPyP in MeOH shows a fluorescence band red-shifting in position and decreasing in intensity, which is mainly due to the lamellar aggregation of TAzoPyP in MeOH (Figs. S19-S20, see ESI†). Besides, both of

the TAzoPyP and its supramolecular nanoparticles exhibit nearly equal fluorescence intensity. Meanwhile, it is worth noting that the remarkable fluorescence decrease in intensity of these two water-soluble nanoparticles might be attributed to either photo-induced electron transfer from the electronically excited porphyrin to an Azo group,[18] or aggregation-induced fluorescence quenching of the porphyrin excited state.[19] Furthermore, the fluorescence quantum yields of TAzoPyP under different conditions with excitation of the porphyrin moiety at 415 nm were determined as shown in Table 1. When TAzoPyP is dissolved in DMSO, a solvent in which TAzoPyP is only minimally aggregated, we observe the fluorescence quantum yield (Φ_{Fl}) ≈ 0.069. For TAzoPyP in MeOH, the Φ_{Fl} is halved to approximate 0.034 due to aggregation-induced fluorescence quenching of TAzoPyP excited state. Nevertheless, both Φ_{Fl} values of TAzoPyP NPs and TAzoPyP/α-CD NPs in water (0.0035 and 0.01, respectively) are significantly smaller than the Φ_{Fl} of TAzoPyP in DMSO, which is consistent with the steady-state fluorescence measurements in Fig. 4c. Additionally, the TAzoPyP/α-CD NPs exhibit higher Φ_{Fl} value than that of TAzoPyP NPs, which might be ascribed to that the aggregation-induced quenching effect has been remarkably restricted by the host-guest interaction between α-CD and TAzoPyP.[20]

Table 1 Fluorescence lifetime and quantum yield of TAzoPyP in different solvents.

Samples	Lifetime (τ) [ns]	Quantum yield (Q_y)[a]
TAzoPyP in DMSO	10.13	0.069
TAzoPyP in MeOH	1.451 (95.9%); 8.261 (4.1%)	0.034
TAzoPyP NPs	4.33	0.0035
TAzoPyP/α-CD NPs	4.558	0.01

[a] TPP was used as the reference.

The time-resolved fluorescence spectra of TAzoPyP samples are given in Fig. 4d. TAzoPyP in DMSO with 415 nm excitation yields a decay best fit to a single exponential decay, with a long lifetime (τ_{Fl}) component of 10.13 ns (100%) (Table 1), which is very close to the lifetime of tetraphenylporphyrin (TPP) in THF (Figs. S21-S22, see ESI†). In comparison, TAzoPyP in MeOH gives a long-lived fluorescence component of approximately 8.261 ns (4.1%) and a short-lived component of 1.451 ns (95.9%). Indeed, the lifetime value (8.261 ns) of the long-lived component in MeOH is quite close to that (10.13 ns) of TAzoPyP in DMSO, which indicates that an extremely small amount of TAzoPyP remains unimolecular state in MeOH. Inversely, a large number of lamellar aggregates in MeOH have a very short fluorescence lifetime of 1.451 ns, which can be ascribed to the fluorescence quenching from the H-type π stacks of TAzoPyP. Furthermore, TAzoPyP NPs and TAzoPyP/α-CD NPs in water yield monoexponential fluorescence decays, having a lifetime of 4.33 ns and 4.558 ns, respectively. In contrast to TAzoPyP in DMSO, the significant decrease in the lifetime could be caused by H-type aggregation of TAzoPyP and spherical nanoparticles formation. On the other hand, the lifetime of these nanoparticles is considerably longer than that of the lamellar aggregates in MeOH, and the difference in the lifetime between these two assemblies mainly depends on the molecular packing structures in these aggregates. As a result, the delocalization of the excited-state energy over several porphyrin units in the assembly and energy migration through the assembly has an important effect on the lifetime of the assembly.[21]

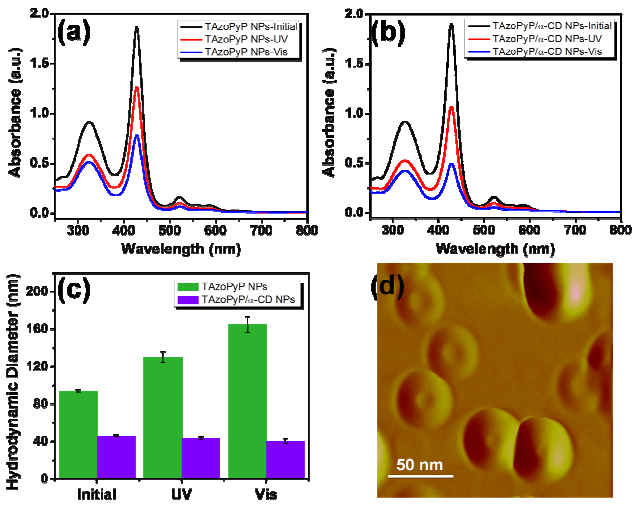

Fig. 5. UV-Vis spectra of (a) TAzoPyP NPs and (b) TAzoPyP/α-CD NPs (c = 10 μM) at the initial state, after UV-365 irradiation for 5 min and after Vis-450 irradiation for 10 min. (c) The hydrodynamic diameter variation of TAzoPyP NPs and TAzoPyP/α-CD NPs by UV-365 or Vis-450 irradiation. (d) AFM image of TAzoPyP/α-CD NPs after irradiation for several minutes using incandescent light.

Another potentially useful property of the resulting porphyrin-based amphiphile is their ability to respond mechanically to light illumination. In Fig. S23 (see ESI†), the unimolecular TAzoPyP in DMSO shows reversible photoisomerization for the azobenzene moiety along with irreversible photobleaching phenomenon for the porphyrin group upon alternating irradiation with UV and Vis light. In comparison, the TAzoPyP nanosheets in MeOH could hardly respond to UV and Vis light illumination as shown in Fig. S24 (see ESI†). We note that the TEtPyP in water could not respond to light illumination (Fig. S25, see ESI†), whereas the TAzoPyP NPs and TAzoPyP/α-CD NPs in water exhibit significant variations in size, morphology and optical properties in response to light (Fig. 5). Figs. 5a,b demonstrate the absorption bands of TAzoPyP NPs and TAzoPyP/α-CD NPs significantly decrease after being irradiated with UV and Vis light, which might be attributed to the photobleaching of porphyrin molecule.[22] In Fig. 5c, the hydrodynamic diameter of TAzoPyP NPs gradually increases from ca. 90 nm to ca. 165 nm upon alternative UV and Vis light illumination. By comparison, the TAzoPyP/α-CD NPs exhibit much higher stability than that of TAzoPyP NPs, so that the hydrodynamic diameter of TAzoPyP/α-CD NPs still remains constant at ca. 46 nm in response to light illumination.

Furthermore, the TAzoPyP/α-CD NPs exhibit reversible change in morphology. As depicted in Fig. 5d, irradiation of TAzoPyP/α-CD NPs using incandescent light results in the formation of concave structures. This response to light is reversible, thus the convex nanoparticles can reform when left in the dark for a period of time. The conversion from convex to concave structures suggests a softening of the core-shell nanoparticles and a collapse of the nanoparticle structure, probably as a result of photo-initiated intermolecular electron

transfer that disrupts the charge balance and the rigidity of the structure[8a,18] as well as *trans*-to-*cis* photoisomerization of azobenzene group,[23] leading to molecular rearrangement of TAzoPyP and collapse of the stacked structure. The softening effect might be attributed to local heating from energy relaxation of the photo-excited porphyrin molecules.

In summary, we have reported a porphyrin-based amphiphile that exhibits various self-assembled morphologies in different solvents. Furthermore, the effect of aggregated structure on optical properties of this amphiphile has been well investigated to get a better understanding on the relationship between structure and properties. In addition, this porphyrin-based amphiphile and its assemblies show dynamic/reversible variations in morphology and optical properties in response to light. It is expected that the resulting water-soluble spherical nanoparticles from this porphyrin-based amphiphile can be used *in vitro* as a potential photosensitizing agent for photodynamic therapy.

Acknowledgements

This work is sponsored by the National Basic Research Program (2012CB821500, 2013CB834506), the Open Project of State Key Laboratory of Chemical Engineering (SKL-ChE-12C04), China National Funds for Distinguished Young Scientists (21025417) and the National Natural Science Foundation of China (21374062, 21204048). R. J. Dong gratefully acknowledges the Scholarship Award for Excellent Doctoral Student granted by Ministry of Education.

Notes and references

[a] *School of Chemistry and Chemical Engineering, State Key Laboratory of Metal Matrix Composites, Shanghai Jiao Tong University, 800 Dongchuan Road, 200240 Shanghai, P. R. China. E-mail: xyzhu@sjtu.edu.cn; +86-21-34203400.*

[b] *Instrumental Analysis Center, Shanghai Jiao Tong University, 800 Dongchuan Road, Shanghai 200240, P. R. China*

[c] *Department of Chemical and Biomolecular Engineering, University of California, Los Angeles, California 90095, United States. E-mail: luucla@ucla.edu*

† Electronic Supplementary Information (ESI) available: Exeriemntal details and characterization data. See DOI: 10.1039/b000000x/

§ Joint first author.

1 (*a*) T. J. Marks, *Science*, 1985, **227**, 881–889; (*b*) S. Fukuzumi and T. Kojima, *J. Mater. Chem.*, 2008, **18**, 1427–1439; (*c*) C. M. Drain, A. Varotto and I. Radivojevic, *Chem. Rev.*, 2009, **109**, 1630–1658; (*d*) C. J. Medforth, Z. Wang, K. E. Martin, Y. Song, J. L. Jacobsen and J. A. Shelnutt, *Chem. Commun.*, 2009, **45**, 7261–7277.

2 (*a*) T. van der Boom, R. T. Hayes, Y. Zhao, P. J. Bushard, E. A. Weiss and M. R. Wasielewski, *J. Am. Chem. Soc.*, 2002, **124**, 9582–9590; (*b*) X. Gong, T. Milic, C. Xu, J. D. Batteas and C. M. Drain, *J. Am. Chem. Soc.*, 2002, **124**, 14290–14291; (*c*) S. Tomas and L. Milanesi, *J. Am. Chem. Soc.*, 2009, **131**, 6618–6623; (*d*) B.-W. Liu, Y. Chen, B.-E Song and Y. Liu, *Chem. Commun.*, 2011, **47**, 4418–4420.

3 (*a*) J. F. Lovell, C. S. Jin, E. Huynh, H. Jin, C. Kim, J. L. Rubinstein, W. C. W. Chan, W. Cao, L. V. Wang and G. Zheng, *Nat. Mater.*, 2011, **10**, 324–332; (*b*) K. J. Son, H.-J. Yoon, J.-H. Kim, W.-D. Jang, Y. Lee and W.-G. Koh, *Angew. Chem. Int. Ed.*, 2011, **50**, 11968–11971; (*c*) X. Liang, X. Li, X. Yue and Z. Dai, *Angew. Chem. Int. Ed.*, 2011, **50**, 11622–11627.

4 (*a*) Z. Wang, Z. Li, C. J. Medforth and J. A. Shelnutt, *J. Am. Chem. Soc.*, 2007, **129**, 2440–2441; (*b*) Y. Tian, C. M. Beavers, T. Busani, K. E. Martin, J. L. Jacobsen, B. Q. Mercado, B. S. Swartzentruber, F. van Swol, C. J. Medforth and J. A. Shelnutt, *Nanoscale*, 2012, **4**, 1695–1700.

5 (*a*) A. D. Schwab, D. E. Smith, C. S. Rich, E. R. Young, W. F. Smith and J. C. de Paula, *J. Phys. Chem. B*, 2003, **107**, 11339–11345; (*b*) A. D. Schwab, D. E. Smith, B. Bond-Watts, D. E. Johnston, J. Hone, A. T. Johnson, J. C. de Paula and W. F. Smith, *Nano Lett.*, 2004, **4**, 1261–1265; (*c*) Y. Liu, C.-F. Ke, H.-Y. Zhang, J. Cui and F. Ding, *J. Am. Chem. Soc.*, 2008, **130**, 600–605.

6 (*a*) Z. Wang, K. J. Ho, C. J. Medforth and J. A. Shelnutt, *Adv. Mater.*, 2006, **18**, 2557–2560; (*b*) A. Tsuda1, Y. Nagamine, R. Watanabe, Y. Nagatani, N. Ishii and T. Aida, *Nat. Chem.*, 2010, **2**, 977–983; (*c*) M. Fathalla, A. Neuberger, S.-C. Li, R. Schmehl, U. Diebold and J. Jayawickramarajah, *J. Am. Chem. Soc.*, 2010, **132**, 9966–9967.

7 S. Yoshimoto, K. Sato, S. Sugawara, Y. Chen, O. Ito, T. Sawaguchi, O. Niwa and K. Itaya, *Langmuir*, 2007, **23**, 809–816.

8 (*a*) Z. Wang, C. J. Medforth and J. A. Shelnutt, *J. Am. Chem. Soc.*, 2004, **126**, 15954–15955; (*b*) S. Tu, S. H. Kim, J. Joseph, D. A. Modarelli and J. R. Parquette, *J. Am. Chem. Soc.*, 2011, **133**, 19125–19130.

9 K. E. Martin, Z. Wang, T. Busani, R. M. Garcia, Z. Chen, Y. Jiang, Y. Song, J. L. Jacobsen, T. T. Vu, N. E. Schore, B. S. Swartzentruber, C. J. Medforth and J. A. Shelnutt, *J. Am. Chem. Soc.*, 2010, **132**, 8194–8201.

10 K. Liu, Y. Liu, Y. Yao, H. Yuan, S. Wang, Z. Wang and X. Zhang, *Angew. Chem. Int. Ed.*, 2013, **52**, 8285–8289.

11 H. A. Benesi and J. H. Hildebrand, *J. Am. Chem. Soc.*, 1949, **71**, 2703–2707.

12 (*a*) J. B. Birks, Photophysics of Aromatic Molecules, Wiley, London, 1970; (*b*) W. I. Gruszecki, *J. Biol. Phys.*, 1991, **18**, 99–109.

13 C. M. Drain, A. Varotto and I. Radivojevic, *Chem. Rev.*, 2009, **109**, 1630–1658.

14 (*a*) L. Yang, N. Takisawa, T. Kaikawa and K. Shirahama, *Langmuir*, 1996, **12**, 1154–1158; (*b*) Y. Liu, Y. Zhao, H. Zhang, Z. Fan, G. Wen and F. Ding, *J. Phys. Chem. B*, 2004, **108**, 8836–8843.

15 G. Pescitelli, S. Gabriel, Y. K. Wang, J. Fleischhauer, R. W. Woody and N. Berova, *J. Am. Chem. Soc.*, 2003, **125**, 7613–7614.

16 (*a*) R. J. Dong, B. S. Zhu, Y. F. Zhou, D. Y. Yan and X. Y. Zhu, *Angew. Chem. Int. Ed.*, 2012, **51**, 11633–11637; (*b*) R. J. Dong, B. S. Zhu, Y. F. Zhou, D. Y. Yan and X. Y. Zhu, *Polym. Chem.*, 2013, **4**, 912–915.

17 R. J. Dong, Y. Liu, Y. F. Zhou, D. Y. Yan and X. Y. Zhu, *Polym. Chem.*, 2011, **2**, 2771–2774.

18 (*a*) M. P. Irvine, R. J. Harrison, G. S. Beddard, P. Leighton, J. K. M. Sanders, *Chem. Phys.*, 1986, **104**, 315–324; (*b*) M. D. Ward, *Chem. Soc. Rev.*, 1997, **26**, 365–375; (*c*) X. Q. Li, M. Wang, S. P. Zhang, J. X. Pan, Y. Na, J. H. Liu, B. Åkermark and L. C. Sun, *J. Phys. Chem. B*, 2008, **112**, 8198–8202.

19 (*a*) N. C. Maiti, S. Mazumdar and N. Periasamy, *J. Phys. Chem. B*, 1998, **102**, 1528-1538; (*b*) N. Serpone and R. F. Khairutdinov, *J. Phys. Chem. B*, 1999, **103**, 761–769; (*c*) Y. Ishida, T. Shimada, H. Tachibana, H. Inoue and S. Takagi, *J. Phys. Chem. A*, 2012, **116**, 12065−12072.

20 (*a*) R. J. Dong, L. Z. Zhou, J. L. Wu, C. L. Tu, Y. Su, B. S. Zhu, H. C. Gu, D. Y. Yan and X. Y. Zhu, *Chem. Commun.*, 2011, **47**, 5473–5475; (*b*) R. J. Dong, H. Y. Chen, D. L. Wang, Y. Y. Zhuang, L. J. Zhu, Y. Su, D. Y. Yan and X. Y. Zhu, *ACS Macro Lett.*, 2012, **1**, 1208−1211; (*c*) R. J. Dong, Y. Su, S. R. Yu, Y. F. Zhou, Y. F. Lu and X. Y. Zhu, *Chem. Commun.*, 2013, **49**, 9845−9847.

21 H. Shao, J. Seifert, N. C. Romano, M. Gao, J. J. Helmus, C. P. Jaroniec, D. A. Modarelli and J. R. Parquette, *Angew. Chem. Int. Ed.*, 2010, **49**, 7688–7691.

22 (*a*) J. D. Spikes, *Photochem Photobiol.*, 1984, **39**, 797–808; (*b*) T. S. Mang, T. J. Dougherty, W. R. Potter, D. G. Boyle, S. Somer and J. Moan, *Photochem Photobiol.*, 1987, **45**, 501–506; (*c*) R. Bonnett, B. D. Djelal, P. A. Hamilton, G. Martinez and F. Wierrani, *J. Photochem. Photobiol. B*, 1999, **53**, 136–143.

23 (*a*) W. Su, H. Zhao, Z. Wang, Y. M. Li and Q. J. Zhang, *Eur. Polym. J.*, 2007, **43**, 657–662; (*b*) D. R. Wang, G. Ye and X. G. Wang, *Macromol. Rapid Commun.*, 2007, **28**, 2237–2243.